第 49 卷第 6 期　　硅　酸　盐　学　报　　Vol. 49，No. 6
2021 年 6 月　　JOURNAL OF THE CHINESE CERAMIC SOCIETY　　June，2021
http://www.gxyb.cbpt.cnki.net　　DOI：10.14062/j.issn.0454-5648.20200754

$CoNiO_2/Ti_3C_2T_x$复合材料的制备及其电化学性能

苏兴华，韩晨曦，张　静，王振军

(长安大学材料科学与工程学院，西安 710061)

摘　要：采用共沉淀方法并结合热处理技术制备了 $CoNiO_2/Ti_3C_2T_x$ 复合材料。使用扫描电子显微镜、X 射线衍射、X 射线光电子能谱、氮气吸脱附测试、循环伏安法、恒流充放电法和电化学阻抗测试对所制备样品进行表征。结果表明：$CoNiO_2/Ti_3C_2T_x$ 质量比为 30:1 的复合材料具有最佳的电化学性能，在 1 A/g 的电流密度下具有 389 F/g 的比电容，约为 $Ti_3C_2T_x$ 比电容的 6 倍；当电流密度为 20 A/g 时，其比电容为 309 F/g；在电流密度为 10 A/g 时，经过 1 500 次充放电循环后，电容保持率为 82%。

关键词：复合材料；电极；超级电容器；二维碳化钛
中图分类号：TB383　　**文献标志码：**A　　**文章编号：**0454–5648(2021)06–1033–08
网络出版时间：2021–04–06

Preparation and Electrochemical Performance of $CoNiO_2/Ti_3C_2T_x$ Composites

SU Xinghua, *HAN Chenxi*, *ZHANG Jing*, *WANG Zhenjun*
(School of Materials Science and Engineering, Chang′an University, Xi′an 710061, China)

Abstract: $CoNiO_2/Ti_3C_2T_x$ composite was prepared by a facile co-precipitation method and subsequent heat treatment. The as-prepared samples were characterized by scanning electron microscopy, X-ray diffraction, X-ray photoelectron spectroscopy, nitrogen adsorption–desorption measurement, cyclic voltammetry, galvanostatic charge–discharge and electrochemical impedance spectroscopy. The results demonstrate that $CoNiO_2/Ti_3C_2T_x$ composite with a $CoNiO_2$:$Ti_3C_2T_x$ mass ratio of 30:1 exhibits the optimum electrochemical performance. The specific capacitance of $CoNiO_2/Ti_3C_2T_x$ composite is 389 F/g at a current density of 1 A/g, which is approximately 6 times greater than that of $Ti_3C_2T_x$. $CoNiO_2/Ti_3C_2T_x$ composite has the specific capacitance of 309 F/g when the current density increases to 20 A/g, and shows a cycle stability with 82% capacitance retention after 1 500 charge–discharge cycles at a current density of 10 A/g.

Keywords: composites; electrodes; supercapacitors; two-dimensional titanium carbide

1　Introduction

With ever-increasing demands in electric energy storage for electric vehicles and modern consumer electronics, supercapacitors have attracted tremendous attentions owing to their high power density, rapid charge/discharge process, high efficiency, good security, wide range of working temperature and long cycle life[1–6]. In general, the electrochemical performance of supercapacitors is greatly influenced by the electrode materials. Therefore, extensive research efforts have been making for developing electrode materials with excellent electrochemical properties[7].

In recent years, a new family of two-dimensional early transition metal carbides and nitrides materials called MXenes has been extensively investigated as electrode materials because they possess metallic conductivity, hydrophilicity and low ions diffusion barrier[8–11]. However, the instinct low specific capacity and re-stacking structure of MXenes limit their further development and practical applications[12–13]. In view of these issues, many studies have focused on adding second phase into MXenes to synthesize composite materials, aiming to improve storage performance and suppress the re-stacking[14–16]. For instance, Levitt *et al*[14]. prepared $Ti_3C_2T_x$ MXene/carbon nanofiber

收稿日期：2020–10–12。　修订日期：2020–11–12。
基金项目：陕西省重点研发计划项目(2019GY-174)。
第一作者：苏兴华(1981—)，博士，教授。

Received date: 2020–10–12.　**Revised date:** 2020–11–12.
First author: SU Xinghua (1981–), male, Ph.D., Professor.
E-mail: suxinghua@chd.edu.cn

composite electrodes, which displayed an areal capacitance of 205 mF/cm^2 at scan rate of 50 mV/s. Zhu *et al*[15]. prepared expanded MXene by using MgO nanoparticles as hard templates, and the obtained composite material displayed a relatively high capacitance of 180 F/g at current density of 1 A/g. Xia *et al*[16]. synthesized BiOCl/$Ti_3C_2T_x$ composites, which showed a remarkably volumetric specific capacitance of 396.5 F/cm^3 at current density of 1 A/g. Although these strategies have improved the capacity of MXenes, the specific capacitance of MXene-based composites are still not high enough for high-performance supercapacitors. Therefore, the new MXene-based composites with high capacitive storage performance need to be further explored.

Due to the high theoretical capacity and good conductivity, binary transition metal oxides as electrode materials for supercapacitors have attracted broad attentions[17–19]. Currently, as an important member of the binary transition metal oxides, $CoNiO_2$ with a special rock salt structure has been focused because of its unique electrochemical properties, economical production process and abundant resources[20–21]. For example, Wang *et al*[20]. fabricated flower-like $NiCoO_2$ spheres via solvothermal process and heat treatment, which delivered a large specific capacitance of 854.9 F/g at 1 A/g. Fan *et al*[21]. prepared mesoporous $CoNiO_2$ hexagonal nanoparticles by a hydrothermal microwave carbon bath method, exhibiting a high capacitance of 801 F/g at 0.5 A/g. In order to promote the electrochemical properties of MXenes electrode materials, introducing $CoNiO_2$ into MXenes and thereby preparation of $CoNiO_2/Ti_3C_2T_x$ composites are expected to be an effective strategy.

In this work, we prepared the $CoNiO_2/Ti_3C_2T_x$ composites using a facile co-precipitation method followed by calcination process. Due to the combination of outstanding conductivity of $Ti_3C_2T_x$ and excellent specific capacitance of $CoNiO_2$, $CoNiO_2/Ti_3C_2T_x$ composites exhibit the superior electrochemical performance. In addition, it is found that the content of $CoNiO_2$ has a great influence on the electrochemical performance of $CoNiO_2/Ti_3C_2T_x$ composites. The specific capacitance can be reached up to 389 F/g at current density of 1 A/g for the 2-$CoNiO_2/Ti_3C_2T_x$ composite with a $CoNiO_2/Ti_3C_2T_x$ mass ratio of 30:1, which is about six times that of the $Ti_3C_2T_x$. Moreover, the 2-$CoNiO_2/Ti_3C_2T_x$ composite shows an excellent rate capability with specific capacitance of 309 F/g when the current density increases up to 20 A/g. This work presents a facile method for preparing MXene-based electrode materials with outstanding electrochemical performance for supercapacitors.

2 Experimental

2.1 Preparation of $CoNiO_2/Ti_3C_2T_x$ composites

The $Ti_3C_2T_x$ MXene was prepared by etching the Ti_3AlC_2 powder with hydrofluoric acid, which was described in our previous work[11]. The $CoNiO_2/Ti_3C_2T_x$ composites were prepared using a co-precipitation method followed by calcination process. Firstly, 10 mg $Ti_3C_2T_x$ MXene was dispersed in 20 mL deionized water with vigorous stirring and ultrasonic treatment for 30 min and a well-mixed suspension was obtained. Afterwards, 1 mmol $Co(NO_3)_2·6H_2O$ and 1 mmol $Ni(CH_3COO)_2·6H_2O$ were dissolved into the above mixed suspension with vigorous stirring for 30 min. Then, 1 mol/L $NH_3·H_2O$ was added slowly into the mixed suspension until pH=10. The obtained products were collected by filtrating, rinsed with deionized water for several times and dried at 180 ℃ for 2 h in a vacuum oven. Finally, the dried products were calcined at 300 ℃ for 2 h in nitrogen. The obtained composite with a $CoNiO_2/Ti_3C_2T_x$ mass ratio of about 15:1 was denoted as 1-$CoNiO_2/Ti_3C_2T_x$ sample.

To investigate the influence of $CoNiO_2$ content on the electrochemical performance of $CoNiO_2/Ti_3C_2T_x$ composite, the $CoNiO_2/Ti_3C_2T_x$ composites with the mass ratio of 30:1, 45:1 and 60:1 were prepared by changing the amount of $CoNiO_2$ and fixing the amount of $Ti_3C_2T_x$ at 10 mg, which were termed as 2-$CoNiO_2/Ti_3C_2T_x$, 3-$CoNiO_2/Ti_3C_2T_x$ and 4-$CoNiO_2/Ti_3C_2T_x$ samples, respectively.

2.2 Materials characterizations

The crystalline structure of as-prepared composites was examined using an X-ray diffractometer (XRD, Bruker D8 Davinci) with Cu K_α radiation. Field-emission scanning electron microscopy (SEM, Hitachi S-4800) was utilized to observe the morphology of as-prepared $CoNiO_2/Ti_3C_2T_x$ composites at an accelerating voltage of 200 kV. The X-ray photoelectron spectroscopy (XPS) of composite was measured by a VG ESCALab 250 equipped with an Al K_α X-ray source. The nitrogen adsorption/desorption measurements were conducted on a QuadraSorb Station 4 at 77 K.

2.3 Electrochemical measurements

Electrochemical measurements were performed on a CHI 660E electrochemical workstation (CH Instruments, Shanghai, China) using three-electrode system. Platinum foil, aqueous saturated calomel electrode (SCE) and 6 mol/L KOH solution were used as the counter electrode, reference electrode and electrolyte, respectively. Electrochemical impedance spectroscopy (EIS) was conducted at open circuit potential with sinusoidal signal of 5 mV between 10 mHz to 100 kHz.

Working electrode was prepared through coating the slurry composed by the $CoNiO_2/Ti_3C_2T_x$ composite, acetylene black and polytetrafluoroethylene (PTFE) with a mass ratio of 8:1:1 on nickel foam (1 cm×1 cm), followed by vacuum drying at 60 ℃ overnight. Based on the galvanostatic charge-discharge (GCD) curve, the specific capacitance was calculated using Eq. (1):

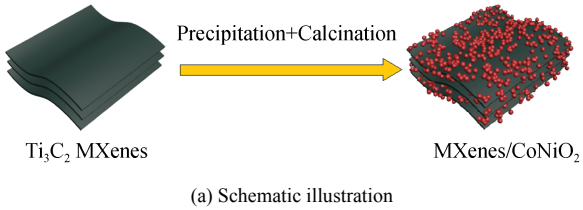
$$C_s = \frac{I\Delta t}{m\Delta V} \quad (1)$$

where C_s (F/g) represented the specific capacitance; I (A) was the discharge current; Δt (s) was the discharge time;

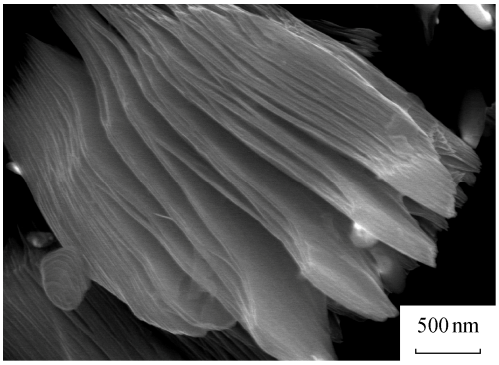
m (g) was the mass of active material, and ΔV (V) was the voltage range.

3 Results and discussion

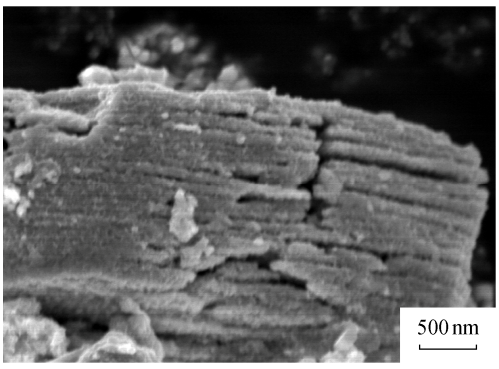
The preparation process of $CoNiO_2/Ti_3C_2T_x$ composite is schematically illustrated in Fig. 1(a). Initially, $Ti_3C_2T_x$ MXene was prepared by etching Al atom layers from Ti_3AlC_2 using HF as an etching reagent. When the Al atom layers are eliminated, surfaces of Ti_3C_2 layers are terminated with functional groups, such as –O, –F or –OH[22]. During the co-precipitation process, these hydrophilic functional groups on the surface of $Ti_3C_2T_x$ MXene can coordinate with Ni^{2+} and Co^{2+} ions, contributing to the nucleation of Ni-Co precursors. After the subsequent calcination, the Ni–Co precursors are transformed into $CoNiO_2$. Fig. 1(b) shows the SEM image of the as-prepared $Ti_3C_2T_x$ MXene using the etching method, which displays the typical accordion-like morphology. The SEM image of the 2-$CoNiO_2/Ti_3C_2T_x$ composite is shown in Fig. 1(c). It can be observed that $CoNiO_2$ nanoparticles are coated uniformly on the surface of $Ti_3C_2T_x$ MXene.



(a) Schematic illustration



(b) $Ti_3C_2T_x$



(c) 2-$CoNiO_2/Ti_3C_2T_x$ composite

Fig. 1 Schematic illustration of synthesis of $CoNiO_2/Ti_3C_2T_x$ composites and SEM images of samples

To characterize the crystalline structure of as-prepared composites, the XRD patterns of $Ti_3C_2T_x$ MXene and $CoNiO_2/Ti_3C_2T_x$ composites with various weight ratios are measured and shown in Fig. 2. Obviously, the diffraction pattern of $Ti_3C_2T_x$ MXene exhibits the characteristic diffraction peaks of (002), (004), (006), (008), and (110) at 2θ=8.84°, 18.23°, 28.03°, 34.32° and 60.56°, respectively, implying a high purity of $Ti_3C_2T_x$ MXene.[12] For the $CoNiO_2/Ti_3C_2T_x$ composites, the diffraction peaks at 2θ=36.66°, 42.73° and 61.94° correspond to the (111), (200) and (220) planes of $CoNiO_2$ (JCPDS 10-0188). Besides the diffraction peaks of $CoNiO_2$, the (002) diffraction peak of $Ti_3C_2T_x$ can also be observed, indicating that $CoNiO_2/Ti_3C_2T_x$ composites are successfully prepared. Furthermore, the position of (002) $Ti_3C_2T_x$ diffraction peak shifts toward to lower 2θ angle of 5.88°, meaning the expansion of the interlayer spacing of $Ti_3C_2T_x$, which may result from the intercalation of Co, Ni atoms or $CoNiO_2$ nanoparticles. In addition, there is no obvious change in the diffraction patterns of $CoNiO_2/Ti_3C_2T_x$ composites with the increase of $CoNiO_2$ content, revealing the high purity of samples.

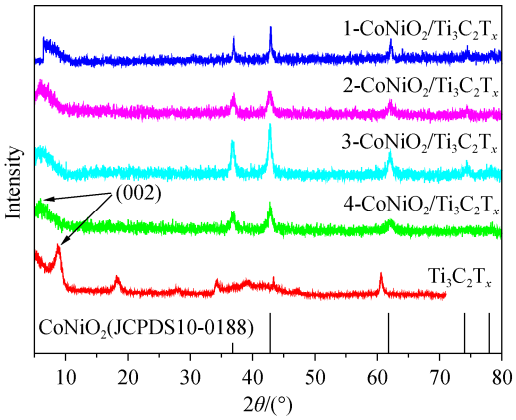
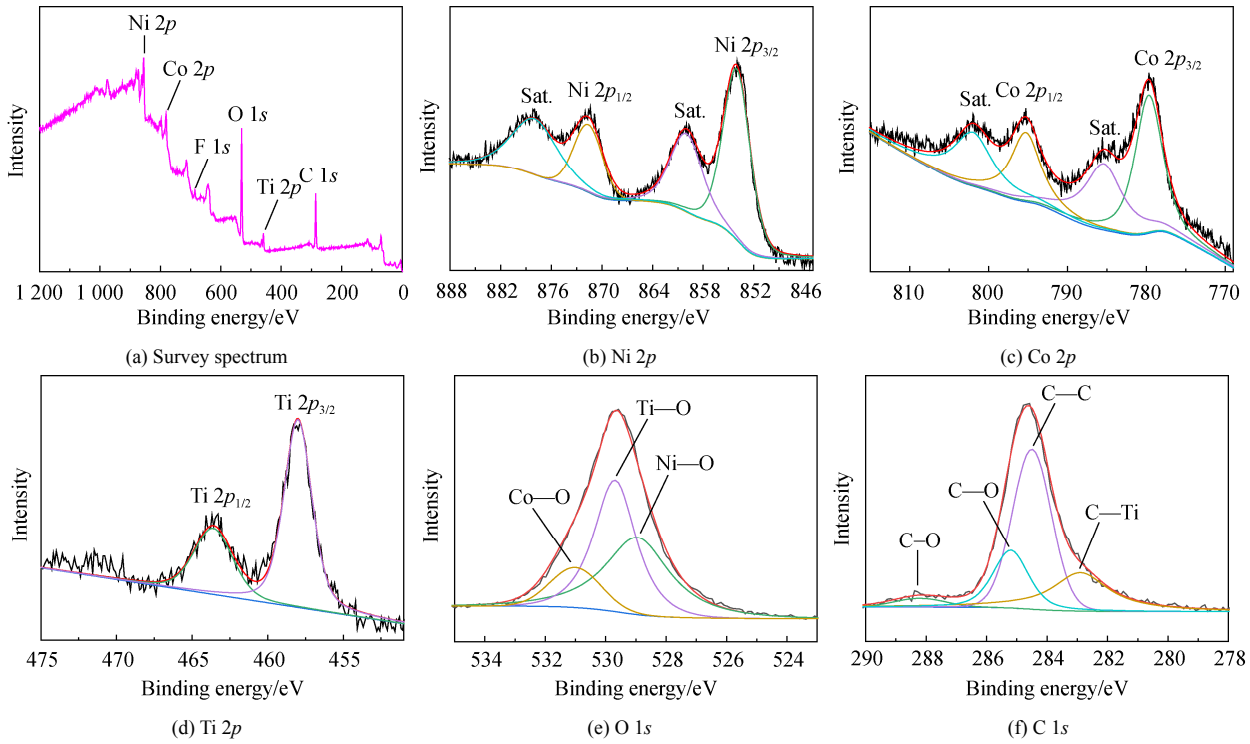


Fig. 2 XRD patterns of $CoNiO_2/Ti_3C_2T_x$ composites and $Ti_3C_2T_x$

The XPS survey spectrum of the 2-$CoNiO_2/Ti_3C_2T_x$ composite is shown in Fig. 3(a). It shows the signals of Co, Ni, O, Ti, C and F elements, further demonstrating the successful preparation of the $CoNiO_2/Ti_3C_2T_x$ composite. It should be noted that the signal of F element comes from the F termination of Ti_3C_2 surfaces. Fig. 3(b) displays the high resolution spectrum of Ni 2*p*. The main peaks at ~854.2 eV and ~871.7 eV are assigned to the Ni $2p_{3/2}$ and Ni $2p_{1/2}$, respectively. The shoulder peaks located at about 860.3 eV and 878.6 eV are corresponding satellite peaks of Ni^{2+} (denoted as sat.).[23] Fig. 3(c) presents the high resolution spectrum of Co 2*p*, which can be deconvoluted into four peaks. The main peaks located at ~779.6 eV and ~795.4 eV are ascribed to the Co $2p_{3/2}$ and Co $2p_{1/2}$, respectively. The shoulder peaks at ~785.2 eV and ~802.2 eV are satellite peaks of Co^{2+}.[20] The Ti 2*p* spectrum shown in Fig. 3(d) can be

deconvolved into two peaks at 458.1 eV and 463.7 eV, which can be assigned to the Ti $2p_{3/2}$ and Ti $2p_{1/2}$, respectively.[12] As for the O 1*s* spectrum shown in Fig. 3(e), the peaks at 528.9, 529.7 eV and 531.1 eV correspond to Ni—O, Ti—O, and Co—O bonds, respectively[24–26]. The high resolution spectrum of C 1*s* is shown in Fig. 3(f). There are four peaks at approximately 281.9, 284.5, 285.2 eV and 288.3 eV can be observed, which is assigned to the C—Ti, C—C, C—O and C=O bonds, respectively[12]. These XPS results further indicate that the $CoNiO_2/Ti_3C_2T_x$ composite is prepared successfully.

The nitrogen adsorption/desorption isotherms of $Ti_3C_2T_x$ and 2-$CoNiO_2/Ti_3C_2T_x$ composite are shown in Fig. 4(a). Both samples exhibit the type IV curves with a H_3 hysteresis loop, implying the presence of mesoporous structure[27], which is further confirmed by the pore size distribution illustrated in Fig. 4(b). Using the Brunauer-Emmett-Teller method, the specific surface area of 2-$CoNiO_2/Ti_3C_2T_x$ composite is calculated to be 41.7 m^2/g, which is larger than that of $Ti_3C_2T_x$ (22.3 m^2/g). This may be attributed to the presence of $CoNiO_2$ nanoparticles and the expansion of the interlayer spacing.

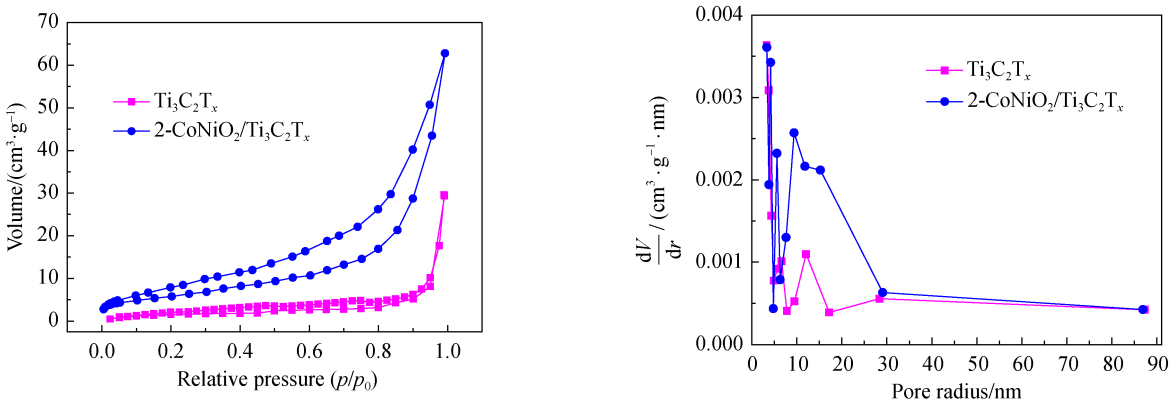


(a) Survey spectrum (b) Ni 2*p* (c) Co 2*p*

(d) Ti 2*p* (e) O 1*s* (f) C 1*s*

Sat. is satellite peaks.

Fig. 3 XPS spectra of the 2-$CoNiO_2/Ti_3C_2T_x$ composite



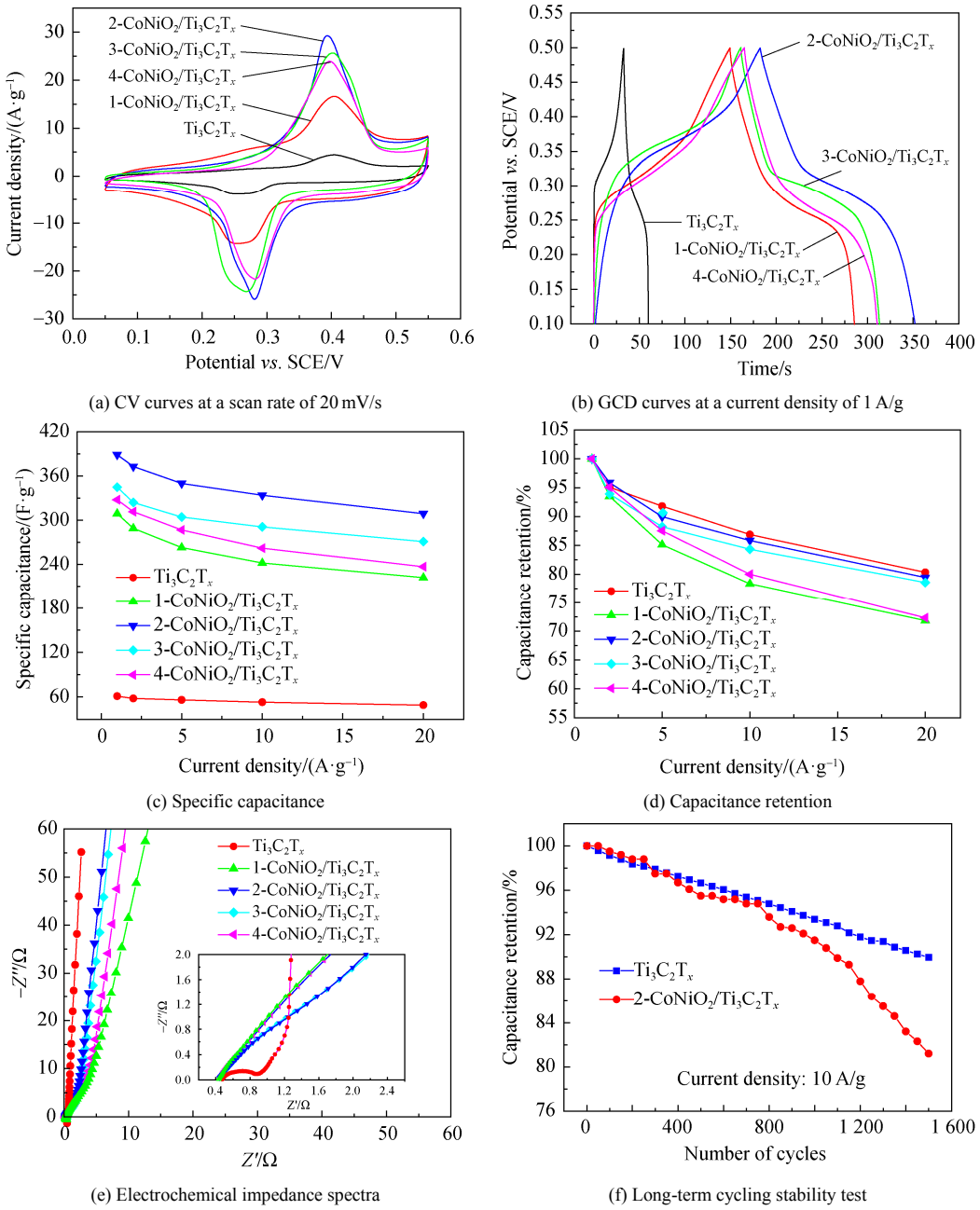
(a) N_2 adsorption/desorption isotherms (b) Pore size distributions

Fig. 4 BET tests of 2-$CoNiO_2/Ti_3C_2T_x$ composite and $Ti_3C_2T_x$

From the Fig. 4(b), it can also be observed that the pore sizes of $Ti_3C_2T_x$ and 2-$CoNiO_2/Ti_3C_2T_x$ composite are in the same range of 2–30 nm. However, the 2-$CoNiO_2/Ti_3C_2T_x$ composite possesses the larger

mesopore volume compared to the $Ti_3C_2T_x$ MXene. It is well known that large surface area and mesoporosity can offer more active sites for electrochemical reactions, and also favor the diffusion of electrolyte ions, thus leading to the enhanced electrochemical properties[28]. Therefore, it is reasonable to expect that the $CoNiO_2/Ti_3C_2T_x$ composites have the superior electrochemical performance in comparison to $Ti_3C_2T_x$ MXene.

Fig. 5(a) shows the cyclic voltammetry (CV) curves of $CoNiO_2/Ti_3C_2T_x$ composites and $Ti_3C_2T_x$ at a scan rate of 20 mV/s. All the samples show the obvious redox peaks, which are caused by the Faradaic redox reactions[29–30]. The pseudocapacitance of $Ti_3C_2T_x$ electrode may be ascribed to the redox reaction involving oxygen-containing functional groups and Ti atoms[31–32]. For the $CoNiO_2/Ti_3C_2T_x$ composites, the capacitance mainly results from the faradaic reactions of $CoNiO_2$ occurring in the alkaline electrolyte, which can be described by Eq. (2)– Eq. (4) [33].



(a) CV curves at a scan rate of 20 mV/s　(b) GCD curves at a current density of 1 A/g

(c) Specific capacitance　(d) Capacitance retention

(e) Electrochemical impedance spectra　(f) Long-term cycling stability test

SCE means saturated calomel electrode.

Fig. 5　Electrochemical tests for $CoNiO_2/Ti_3C_2T_x$ composites and $Ti_3C_2T_x$

$$CoNiO_2 + 2OH^- \leftrightarrow CoOOH + NiOOH + 2e^- \quad (2)$$

$$CoOOH + OH^- \leftrightarrow CoO_2 + H_2O + e^- \quad (3)$$

$$NiOOH + OH^- \leftrightarrow NiO_2 + H_2O + e^- \quad (4)$$

From the CV curves, it can be obviously observed that the enclosed areas of the $CoNiO_2/Ti_3C_2T_x$ composites are much larger than that of $Ti_3C_2T_x$, suggesting that the

$CoNiO_2/Ti_3C_2T_x$ composites possess the higher specific capacitance compared to the $Ti_3C_2T_x$. This is mainly due to the contribution of $CoNiO_2$ which can increase the surface area and thereby offer more active sites for Faradaic reaction. Moreover, it is found that the CV curve of 2-$CoNiO_2/Ti_3C_2T_x$ composite has the largest enclosed area, suggesting that 2-$CoNiO_2/Ti_3C_2T_x$ composite possesses the highest specific capacitance among all the samples. Fig. 5(b) shows the GCD curves of $CoNiO_2/Ti_3C_2T_x$ composites and $Ti_3C_2T_x$ at a current density of 1 A/g. The obvious plateaus in all GCD curves verify the battery-like behavior in $CoNiO_2/Ti_3C_2T_x$ composites[32, 34], which is in accordance with CV results. The $CoNiO_2/Ti_3C_2T_x$ composites exhibit the far longer discharge time than that of $Ti_3C_2T_x$, further confirm the higher specific capacitance of $CoNiO_2/Ti_3C_2T_x$ in comparison to $Ti_3C_2T_x$. Furthermore, the longest discharge time of 2-$CoNiO_2/Ti_3C_2T_x$ implies the highest specific capacitance, which agrees well with the CV results.

According to GCD curves, the specific capacitances of $CoNiO_2/Ti_3C_2T_x$ composites and $Ti_3C_2T_x$ electrodes at different discharge current densities are calculated and given in Fig. 5(c). The $Ti_3C_2T_x$, 1-$CoNiO_2/Ti_3C_2T_x$, 2-$CoNiO_2/Ti_3C_2T_x$, 3-$CoNiO_2/Ti_3C_2T_x$ and 4-$CoNiO_2/Ti_3C_2T_x$ show the specific capacitance of 61, 309, 389, 345 F/g and 328 F/g at the current density of 1 A/g, respectively. Obviously, the $CoNiO_2/Ti_3C_2T_x$ composites exhibit the larger specific capacitance in comparison to the $Ti_3C_2T_x$. Among the composites, the 2-$CoNiO_2/Ti_3C_2T_x$ exhibits the largest specific capacitance of 389 F/g. Moreover, 2-$CoNiO_2/Ti_3C_2T_x$ shows a good rate capability with a specific capacitance of 309 F/g even at the high current density of 20 A/g. Fig. 5(d) shows the capacitance retention as a function of discharge current density for $CoNiO_2/Ti_3C_2T_x$ composites and $Ti_3C_2T_x$. The 2-$CoNiO_2/Ti_3C_2T_x$ demonstrates a high rate capability with 80% capacitance retention at the high current density of 20 A/g.

To further understand the fundamental electrochemical behavior of as-prepared samples, their electrochemical impedance spectroscopies (EIS) are measured. Fig. 5(e) shows the Nyquist plots of $CoNiO_2/Ti_3C_2T_x$ composites and $Ti_3C_2T_x$ MXene. The slope of the line at low frequency corresponds to the Warburg impedance value (R_W), which is related to the electrolyte ion diffusion within electrode[35]. It can be observed that the 2-$CoNiO_2/Ti_3C_2T_x$ composite shows a more vertical line than other composites, implying a lower R_W. These results suggest that the 2-$CoNiO_2/Ti_3C_2T_x$ composite has the low ion diffusion impedance, indicating that the electrolyte ions are easily diffused in the 2-$CoNiO_2/Ti_3C_2T_x$ composite. Nevertheless, the $Ti_3C_2T_x$ shows the lowest R_W in comparison to the $CoNiO_2/Ti_3C_2T_x$ composites. At high frequency region, the intercept at the real axis represents the series resistance (R_s), which corresponds to the intrinsic impedance of the electrode material[24, 35–36]. As depicted in the inset of Fig. 5(e), the R_s of the $Ti_3C_2T_x$, 1-$CoNiO_2/Ti_3C_2T_x$, 2-$CoNiO_2/Ti_3C_2T_x$, 3-$CoNiO_2/Ti_3C_2T_x$ and 4-$CoNiO_2/Ti_3C_2T_x$ is 0.477, 0.438, 0.433, 0.435 Ω and 0.436 Ω, respectively. Clearly, the $CoNiO_2/Ti_3C_2T_x$ composites exhibit the lower R_s than that of $Ti_3C_2T_x$. Among the composites, the 2-$CoNiO_2/Ti_3C_2T_x$ has the lowest R_s, also revealing its excellent electrochemical properties.

Long cycle stability is a key parameter for evaluating electrode materials in high performance supercapacitors. Therefore, 1 500 charge–discharge cycles at a high current density of 10 A/g is carried out for 2-$CoNiO_2/Ti_3C_2T_x$ composite and $Ti_3C_2T_x$. The results demonstrate that the 2-$CoNiO_2/Ti_3C_2T_x$ has the good cycle stability with 82% capacitance retention, as shown in Fig. 5(f). Nevertheless, the $Ti_3C_2T_x$ shows the better cycle stability compared to the 2-$CoNiO_2/Ti_3C_2T_x$. The decay of capacitance for 2-$CoNiO_2/Ti_3C_2T_x$ may come from the detachment of $CoNiO_2$ nanoparticles from the $Ti_3C_2T_x$. The detached $CoNiO_2$ nanoparticles form the dead zones, which can affect the electron and ion transmission rates, thereby reducing charge accumulation and redox reactions. Fig. 6 shows the SEM image of the 2-$CoNiO_2/Ti_3C_2T_x$ composite electrode after 1 500 cycles. It can be seen that the ordered accordion like structure disappears and $CoNiO_2$ nanoparticles are partially detached from the $Ti_3C_2T_x$.

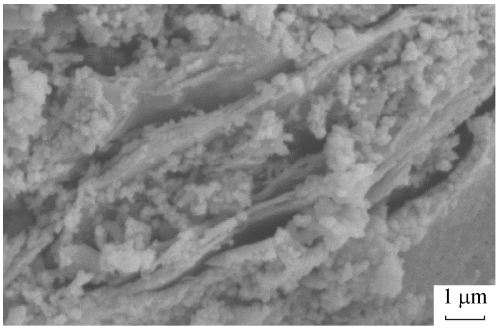
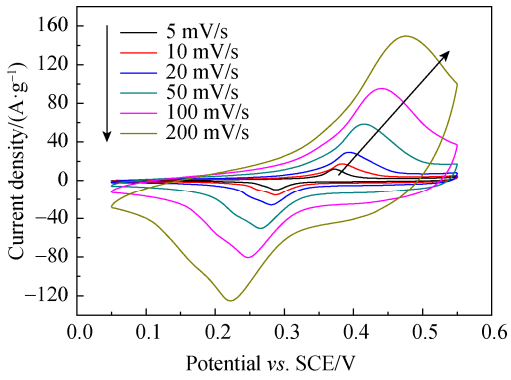


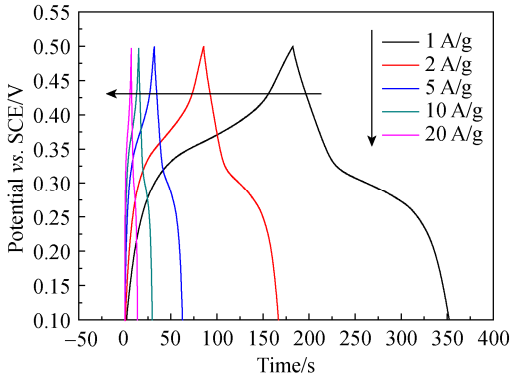
Fig. 6 SEM image of 2-$CoNiO_2/Ti_3C_2T_x$ composite electrode after 1 500 cycles

Because 2-$CoNiO_2/Ti_3C_2T_x$ displays the best capability, rate capability and cycle stability among the $CoNiO_2/Ti_3C_2T_x$ composites, its electrochemical properties are further investigated. The CV analyses at different scan rates in the range of 5–200 mV/s and GCD analyses at various current densities in the range of 1–20 A/g are conducted and corresponding results are displayed in Fig. 7. It is clearly found that the integrated area becomes larger as the scan rate increases, which was shown in Fig. 7(a). All of the CV curves show the obvious redox peaks, implying the typical battery-type characteristics of the 2-$CoNiO_2/Ti_3C_2T_x$[37–38]. The position of the redox peaks shifts slightly to converse direction with increase of the scan rate, possibly resulting from the polarization effect. The similar shape of CV curves at different scan rates indicates the excellent electrochemical reversibility of the 2-$CoNiO_2/Ti_3C_2T_x$[39–40].

The obvious plateaus in all GCD curves shown in Fig. 7(b) further verify the battery-like behavior for 2-$CoNiO_2/Ti_3C_2T_x$[36]. Meanwhile, the nearly symmetric GCD curves at various current densities imply the high rate charge–discharge performance[41]. which is in accordance with the CV results.



(a) CV at different scan rates



(b) GCD at differnet current densities

Fig. 7　CV and GCD for 2-$CoNiO_2/Ti_3C_2T_x$ composite

Clearly, the specific capacitance of the 2-$CoNiO_2/Ti_3C_2T_x$ is higher than those of the $CoNiO_2$ and $Ti_3C_2T_x$ based electrode materials reported in literature, such as $NiCoO_2$ (328.5 F/g at 0.62 A/g) [42], $CNT/Ti_3C_2T_x$ (384 F/g at 10 mV/s) [31], and $TiO_2/Ti_3C_2T_x$ (143 F/g at 5 mV/s) [43]. The enhanced electrochemical properties of $CoNiO_2/Ti_3C_2T_x$ composites can be understood from the following aspects. First, intercalation of Co and Ni atoms or $CoNiO_2$ nanoparticles into interlayers of $Ti_3C_2T_x$ MXene can increase the interlayer spacing, enabling the high capacitance. Second, the attachment of $CoNiO_2$ nanoparticles on the surface of $Ti_3C_2T_x$ provides more active sites for Faradaic redox reaction, further increasing the capacitance. Third, broadened interlayer spacing is beneficial for fast diffusion of electrolyte ions. Fourth, the self-stacking of $Ti_3C_2T_x$ MXene may be efficiently prevented through incorporation of $CoNiO_2$, thereby the electrochemical active sites can be maintained. Due to the enhanced electrochemical performance, $CoNiO_2/Ti_3C_2T_x$ composites could be applied in supercapacitors. In addition, our work presents a facile method to prepare MXene-based electrode materials with excellent electrochemical performance.

4　Conclusions

The $CoNiO_2/Ti_3C_2T_x$ composites are successfully prepared by a facile co-precipitation method followed by heat treatment. The $CoNiO_2/Ti_3C_2T_x$ composites exhibit the superior electrochemical performance. The content of $CoNiO_2$ has a great influence on the electrochemical properties of $CoNiO_2/Ti_3C_2T_x$ composite. The 2-$CoNiO_2/Ti_3C_2T_x$ composite with a $CoNiO_2/Ti_3C_2T_x$ mass ratio of 30:1 shows a high specific capacitance of 389 F/g at current density of 1 A/g, an excellent retention rate with a specific capacitance of 309 F/g at the current density of 20 A/g, and a good cycle stability with 82% retention even at a high current density of 10 A/g after 1 500 charge–discharge cycles.

References:

[1] WU Y, YANG Y, ZHAO X, et al. A novel hierarchical porous 3D structured vanadium nitride/carbon membranes for high-performance supercapacitor negative electrodes[J]. Micro Nano Lett, 2018, 10(4): 63.

[2] SIMON P, GOGOTSI Y, DUNN B. Where do batteries end and supercapacitors begin?[J]. Science, 2014, 343(6176): 1210.

[3] SHAO Y, EL-KADY M F, SUN J, et al. Design and mechanisms of asymmetric supercapacitors[J]. Chem Rev, 2018, 118(18): 9233–9280.

[4] ZHANG D, LI J, SU Z, et al. Electrospun polyporous VN nanofibers for symmetric all-solid-state supercapacitors[J]. J Adv Ceram, 2018, 7(3): 246–255.

[5] MU H, SU X, ZHAO Z, et al. Facile synthesis of $Ni_{0.5}Mn_{0.5}Co_2O_4$ nanoflowers as high-performance electrode material for supercapacitors[J]. J Am Ceram Soc, 2019, 102(11): 6893–6903.

[6] CHEN S, XIANG Y, XU W, et al. A novel MnO_2/MXene composite prepared by electrostatic self-assembly and its use as an electrode for enhanced supercapacitive performance[J]. Inorg Chem Front, 2019, 6(1): 199–208.

[7] YU Z, TETARD L, ZHAI L, et al. Supercapacitor electrode materials: Nanostructures from 0 to 3 dimensions[J]. Energy Environ Sci, 2015, 8(3): 702–730.

[8] LI H, CHEN X, ZALNEZHAD E, et al. 3D hierarchical transition-metal sulfides deposited on MXene as binder-free electrode for high-performance supercapacitors[J]. J Ind Eng Chem, 2020, 82: 309–316.

[9] VENKATESHALU S, GRACE A N. MXenes—A new class of 2D layered materials: Synthesis, properties, applications as supercapacitor electrode and beyond[J]. Appl Mater Today, 2020, 18: 100509.

[10] WANG B, ZHOU A, LIU F, et al. Carbon dioxide adsorption of two-dimensional carbide MXenes[J]. J Adv Ceram, 2018, 7(3): 237–245.

[11] SU X, ZHANG J, MU H, et al. Effects of etching temperature and ball milling on the preparation and capacitance of Ti_3C_2 MXene[J]. J Alloy Compd, 2018, 752: 32-39.

[12] JIANG F, DU R, YAN X, et al. Ferroferric oxide nanoclusters decorated $Ti_3C_2T_x$ nanosheets as high performance anode materials for lithium ion batteries[J]. Electrochim Acta, 2020, 329: 135146.

[13] TAO M, DU G, ZHANG Y, et al. TiOxNy nanoparticles/C composites derived from MXene as anode material for potassium-ion batteries[J]. Chem Eng J, 2019, 369: 828–833.

[14] LEVITT A S, ALHABEB M, HATTER C B, et al. Electrospun

MXene/carbon nanofibers as supercapacitor electrodes[J]. J Mater Chem A, 2019, 7(1): 269–277.
[15] ZHU Y, RAJOUâ K, LE VOT S, et al. Modifications of MXene layers for supercapacitors[J]. Nano Energy, 2020, 73: 104734.
[16] XIA Q X, SHINDE N M, YUN J M, et al. Bismuth oxychloride/MXene symmetric supercapacitor with high volumetric energy density[J]. Electrochim Acta, 2018, 271: 351–360.
[17] LOW W H, KHIEW P S, LIM S S, et al. Recent development of mixed transition metal oxide and graphene/mixed transition metal oxide based hybrid nanostructures for advanced supercapacitors[J]. J Alloy Compd, 2019, 775: 1324–1356.
[18] YASIN A S, MOHAMED A Y, MOHAMED I M A, et al. Theoretical insight into the structure-property relationship of mixed transition metal oxides nanofibers doped in activated carbon and 3D graphene for capacitive deionization[J]. Chem Eng J, 2019, 371: 166–181.
[19] LI J, LIU Z, ZHANG Q, et al. Anion and cation substitution in transition-metal oxides nanosheets for high-performance hybrid supercapacitors[J]. Nano Energy, 2019, 57: 22–33.
[20] WANG Z, ZHAO Z, ZHANG Y, et al. Hierarchical flower-like conductive $CoNiO_2$ microspheres constructed with ultrathin mesoporous nanosheets towards long-cycle-life hybrid supercapacitors[J]. J Alloy Compd, 2019, 779: 81–90.
[21] FAN C, ZHANG X, CHEN L, et al. Preparation of mesoporous $CoNiO_2$ hexagonal nanoparticles for asymmetric supercapacitors *via* a hydrothermal microwave carbon bath process[J]. New J Chem, 2019, 43(38): 15066–15071.
[22] ALHABEB M, MALESKI K, ANASORI B, et al. Guidelines for synthesis and processing of two-dimensional titanium carbide ($Ti_3C_2T_x$ MXene)[J]. Chem Mater, 2017, 29(18): 7633–7644.
[23] CHANG L, WANG K, ZHU S, et al. Facile synthesis of 3D foam-like $CoNiO_2$ for high-performance sodium ion batteries[J]. Mater Res Bull, 2017, 96: 379–384.
[24] LIU Q, YANG J, LUO X, et al. Fabrication of a fibrous MnO_2@MXene/CNT electrode for high-performance flexible supercapacitor[J]. Ceram Int, 2020, 46(8, Part B): 11874–11881.
[25] SUN Y, ZHOU Y, ZHU C, et al. A Pt–Co_3O_4–CD electrocatalyst with enhanced electrocatalytic performance and resistance to CO poisoning achieved by carbon dots and Co_3O_4 for direct methanol fuel cells[J]. Nanoscale, 2017, 9(17): 5467–5474.
[26] SAN CHOI J, AHN C W, BAE J-S, et al. Identifying a perovskite phase in rare-earth nickelates using X-ray photoelectron spectroscopy[J]. Curr Appl Phys, 2020, 20(1): 102–105.
[27] VINU A, SAWANT D P, ARIGA K, et al. Benzylation of benzene and other aromatics by benzyl chloride over mesoporous AlSBA-15 catalysts[J]. Micropor Mesopor Mat, 2005, 80(1): 195–203.
[28] LI X, ZHU J, FANG Y, et al. Hydrothermal preparation of CoO/Ti_3C_2 composite material for lithium-ion batteries with enhanced electrochemical performance[J]. J Electroanal Chem, 2018, 817: 1–8.
[29] HU M, CHENG R, LI Z, et al. Interlayer engineering of $Ti_3C_2T_x$ MXenes towards high capacitance supercapacitors[J]. Nanoscale, 2020, 12(2): 763–771.
[30] ZHAN C, NAGUIB M, LUKATSKAYA M, et al. Understanding the MXene Pseudocapacitance[J]. J Phys Chem Lett, 2018, 9(6): 1223–1228.
[31] YAN P, ZHANG R, JIA J, et al. Enhanced supercapacitive performance of delaminated two-dimensional titanium carbide/carbon nanotube composites in alkaline electrolyte[J]. J Power Sources, 2015, 284: 38–43.
[32] SHAO H, LIN Z, XU K, et al. Electrochemical study of pseudocapacitive behavior of $Ti_3C_2T_x$ MXene material in aqueous electrolytes[J]. Energy Stor Mater, 2019, 18: 456–461.
[33] AI Y, GENG X, LOU Z, et al. Rational synthesis of branched $CoMoO_4$@$CoNiO_2$ core/shell nanowire arrays for all-solid-state supercapacitors with improved performance[J]. ACS Appl Mater Interfaces, 2015, 7(43): 24204–24211.
[34] SRIMUK P, KAASIK F, KRüNER B, et al. MXene as a novel intercalation-type pseudocapacitive cathode and anode for capacitive deionization[J]. J Mater Chem A, 2016, 4(47): 18265–18271.
[35] ZOU R, QUAN H, PAN M, et al. Self-assembled MXene($Ti_3C_2T_x$)/α-Fe_2O_3 nanocomposite as negative electrode material for supercapacitors[J]. Electrochim Acta, 2018, 292: 31–38.
[36] RAKHI R B, AHMED B, ANJUM D, et al. Direct chemical synthesis of MnO_2 nanowhiskers on transition-metal carbide surfaces for supercapacitor applications[J]. ACS Appl Mater Interfaces, 2016, 8(29): 18806–18814.
[37] LU C, LI A, ZHAI T, et al. Interface design based on Ti_3C_2 MXene atomic layers of advanced battery-type material for supercapacitors[J]. Energy Stor Mater, 2020, 26: 472–482.
[38] YANG Q, JIAO T, LI M, et al. In situ formation of $NaTi_2(PO_4)_3$ cubes on Ti_3C_2 MXene for dual-mode sodium storage[J]. J Mater Chem A, 2018, 6(38): 18525–18532.
[39] WU X, HUANG B, WANG Q, et al. High energy density of two-dimensional MXene/NiCo-LDHs interstratification assembly electrode: Understanding the role of interlayer ions and hydration[J]. Chem Eng J, 2020, 380: 122456.
[40] GUO X, ZHANG J, SONG J, et al. MXene encapsulated titanium oxide nanospheres for ultra-stable and fast sodium storage[J]. Energy Stor Mater, 2018, 14: 306–313.
[41] FU J, LI L, YUN J M, et al. Two-dimensional titanium carbide (MXene)-wrapped sisal-Like $NiCo_2S_4$ as positive electrode for high-performance hybrid pouch-type asymmetric supercapacitor[J]. Chem Eng J, 2019, 375: 121939.
[42] ZHANG X, XU Y. The precipitant influence on the electrochemical performance of $NiCoO_2$ nanostructure[J]. Mater Lett, 2017, 189: 78–81.
[43] ZHU J, TANG Y, YANG C, et al. Composites of TiO_2 nanoparticles deposited on Ti_3C_2 MXene nanosheets with enhanced electrochemical performance[J]. J Electrochem Soc, 2016, 163(5): A785–A791.

※ ※ ※ ※ ※ ※ ※ ※ ※ ※ ※



苏兴华(1981 年)，男，长安大学材料科学与工程学院教授，硕士生导师。Journal of Advanced Ceramics 编委，材料研究学会会员，教育部学位中心研究生论文评议专家，陕西省科技项目及高新企业认定评审专家，“中国科技论文在线”在线论文特聘评审专家。先后主持国家自然科学基金、高等学校博士学科点专项科研基金、陕西省自然科学基础研究计划、中国博士后科学基金等科研课题 10 项。在国内外学术刊物上发表研究论文篇 65 篇。主要研究方向为先进陶瓷材料及新型能源材料。